Journal of Solid State Chemistry 184 (2011) 2543–2552

Contents lists available at ScienceDirect

Journal of Solid State Chemistry

journal homepage: www.elsevier.com/locate/jssc

Solubility and microstructure in the pseudo-binary PbTe–Ag_2Te system

Kristin Bergum [a], Teruyuki Ikeda [a,b,*], G. Jeffrey Snyder [a]

[a] Materials Science, California Institute of Technology, 1200 California Blvd., Pasadena, CA 91125, USA
[b] PRESTO, Japan Science and Technology Agency, 4-1-8 Honcho, Kawaguchi, Saitama 332-0012, Japan

ARTICLE INFO

Article history:
Received 16 April 2011
Received in revised form
23 June 2011
Accepted 10 July 2011
Available online 20 July 2011

Keywords:
Solubility
Heat of solution
Precipitates
Diffusion couple
Orientation relationship
Thermoelectrics

ABSTRACT

The solvus lines of the PbTe and Ag_2Te phases in the pseudo-binary PbTe–Ag_2Te system have been determined using diffusion couples and unidirectional solidification by the Bridgman method. The solubilities of both Ag_2Te in PbTe and PbTe in Ag_2Te decrease with decrease in temperature. For the former, this change is from 14.9 at% Ag (694 °C) to 0.5 at% Ag (375 °C), while for the latter it is from 12.4 at% Pb (650 °C) to 3.1 at% Pb (375 °C). The decrease in solubilities leads to the formation of precipitates of Ag_2Te in PbTe and PbTe in Ag_2Te. In particular, fast atomic diffusion in Ag_2Te results in the precipitation of PbTe even in quenched samples. From the temperature dependence of these solubilities, heats of solution have been determined. In the diffusion couple, the phase boundary moves toward PbTe. In the region between the phase boundary and the initial interface, PbTe transforms to β-Ag_2Te (cubic) retaining the cube-on-cube orientation relationship.

1. Introduction

In thermoelectric materials, reducing the thermal conductivity is one of the key ways to improve thermoelectric conversion efficiencies. Microstructure formation with nanometer scales has recently attracted much attention as an effective way to scatter phonons, leading to lattice thermal conductivity reduction [1]. In metals, semiconductors such as thermoelectric materials, and ionic conductors, the electronic [2] or ionic [3] transport properties are largely affected by point defects. The knowledge on phase diagrams is essential for fabrication processes, control of microstructure, practical use at high temperatures, and understanding thermodynamic and point defect properties.

The pseudo-binary PbTe–Ag_2Te system is composed of the excellent thermoelectric materials PbTe and Ag_2Te. The thermoelectric properties in the PbTe-rich region have been investigated both within the solid solution range [4–6] and at compositions exceeding the solubility limit, where the lattice thermal conductivity is significantly reduced due to the formation of Ag_2Te precipitates [7]. The morphological evolution of Ag_2Te precipitates as well as the interfacial structure between the precipitates and the PbTe matrix have also been studied [8]. Ag_2Te is also known for the superionic conduction property [9,10] of the β-phase (cubic, space group: *Fm*-3*m*, 145 °C < *T* < 802 °C [11])[1] and the good thermoelectric properties of both the α-phase [14–17] (monoclinic, space group: $P2_1/c$, *T* < 145 °C [11]) and the β-phase [18,19]. PbTe based materials in the "LAST" (lead–antimony–silver tellurides) system are known for their high thermoelectric figure of merit [20], which originates from their nanodot structures. Recently, the nanodots have been found to be consisting of Ag_2Te inclusions [21]. The pseudo-binary PbTe–Ag_2Te system is also an important constituent of the LAST system, particularly since LAST compositions close to the PbTe–Ag_2Te pseudo-binary line show the highest thermoelectric figure of merit. Regardless of the importance of this system, the solubility ranges in the solid states have not been extensively investigated. Fig. 1 shows the phase diagram of the pseudo-binary PbTe–Ag_2Te system. The maximum existence ranges of both the PbTe and the Ag_2Te phases have been determined to be 11 and 52 at% Ag, respectively, by extrapolation of the solidus lines measured by differential thermal analysis down to the eutectic temperature (694 °C) [22]. While the latest assessment of the phase diagram of this system [23] draws broken lines as unknown for the solvus lines for both PbTe and Ag_2Te phases, there is one measured point at 500 °C for the PbTe side and there are several points for the Ag_2Te side [24].

In this paper, we determine the solvus lines for the dissolution of Ag_2Te in PbTe phase and those of PbTe in Ag_2Te in the pseudo-binary PbTe–Ag_2Te system as functions of temperature using Ag_2Te/PbTe diffusion couples and unidirectional solidification by the Bridgman method. The determination of solvus lines in this system is essential particularly in controlling the precipitation microstructure and knowing the stability of the precipitates at high temperatures, the thermodynamic properties in the solid solution regions, and the compositions of the matrix phases in the precipitation microstructure, which are connected to the point defect structure and hence thermal and electrical properties.

* Corresponding author at: Materials Science, California Institute of Technology, 1200 California Blvd., Pasadena, CA 91125, USA. Fax: +1 626 395 8868.
E-mail address: tikeda@caltech.edu (T. Ikeda).

[1] Note that we denote the middle temperature Ag_2Te phase (145 °C < *T* < 802 °C) as the β-phase throughout this paper though it is sometimes referred to as the α-phase [10–13].

0022-4596/$ - see front matter © 2011 Elsevier Inc. All rights reserved.
doi:10.1016/j.jssc.2011.07.012

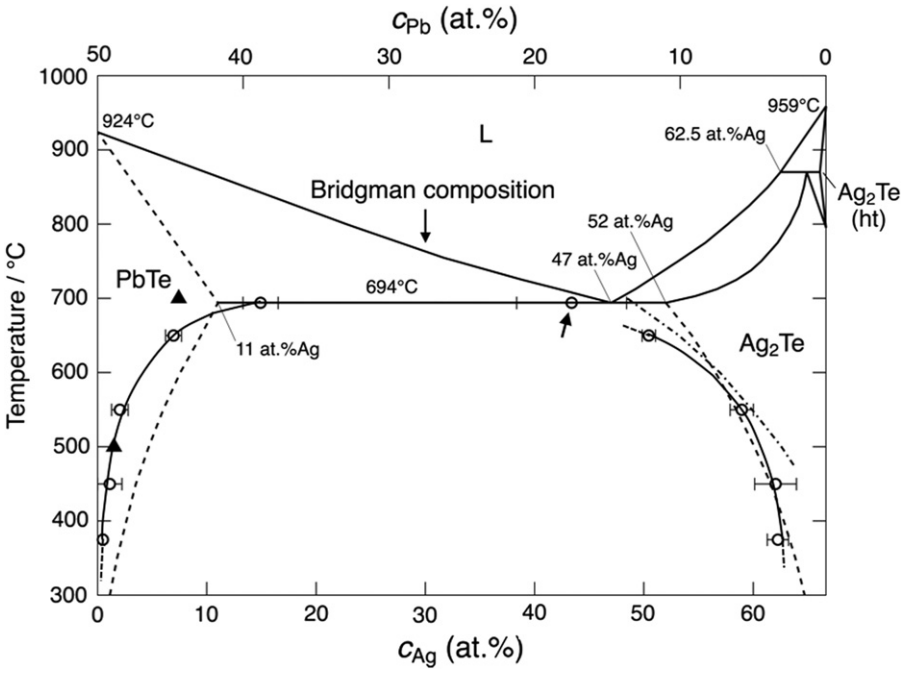

Fig. 1. Phase diagram of the pseudo-binary PbTe–Ag_2Te system. Open circles, for which solid curves are drawn, are the solubility ranges for PbTe and Ag_2Te phases determined in this work. The point with an arrow is the eutectic composition measured from the sample unidirectionally solidified by the Bridgman method. Other solid lines are from the assessment by Grieb [24]. Broken lines were drawn as unknown in Grieb's assessment [24]. Dashed-dotted line and triangles are taken from Wald [25].

2. Experimental

2.1. Diffusion couple experiments.

Ag_2Te and PbTe ingots were synthesized by melting elemental granules of Pb (99.999%, Alfa Aesar), Ag (99.9999%, Alfa Aesar), and Te (99.999%, Alfa Aesar) in carbon coated quartz ampoules filled with 30 kPa of Ar at 950 °C for 10 min. Each ingot weighed 10 g. After melting, the ampoules were quenched in water. They were then annealed at 700 °C for 1 week for homogenization. The homogeneity of the samples was checked by microstructure observation with field emission scanning electron microscopy (FE-SEM, ZEISS 1550 VP).

Diffusion couples between PbTe and Ag_2Te were prepared as follows. The ingots were cut into 3 mm pieces using a low speed diamond saw. One plane of each sample was polished with 9 μm diamond slurry followed by 1 μm slurry on grinding disks to obtain a smooth surface. The polished planes of Ag_2Te and PbTe samples were brought into contact using a stainless steel clamp covered with alumina power. The clamp holding one couple of Ag_2Te and PbTe samples was wrapped in Ti and Ta foil and sealed in a quartz tube with an inner diameter of 22 mm filled with 30 kPa of Ar.

In this study, the phase boundary compositions at various temperatures are determined from the chemical composition profile after annealing at respective temperatures followed by fast cooling. Therefore, the cooling rate must be high enough to retain the chemical composition profiles at the given temperature. In the present system, there were some technical difficulties;

1) PbTe is a fragile material and cooling too fast leads to cracking of the samples,
2) chemical diffusion in this system, especially in Ag_2Te, which is known for its superionic conduction of Ag, is so fast that Ag diffusion during cooling could change the chemical composition profile before cooling if the cooling rate is not high enough, and
3) fast diffusion causes solid state precipitation during cooling, which is due to lower solubilities at lower temperatures. This makes it hard to obtain smooth composition profiles if the microstructure size is too coarse.

Table 1
Annealing conditions and spot size used in EPMA. For methods of quenching, see text.

Sample no	Temperature (°C)	Annealing length	Spot size (μm)	Quenching method
0	375	104 d 20 h	5	3
1	450	8 h	13	1
2		5 d	15	2
3		20 d	20	3
4	550	4 h	13	1
5		16 h	13	3
6		64 h	20	3
7		10 d 16 h	20	3
8	650	1 h	13	1
9		16 h	12	2
10		64 h	20	2
11	Bridgman PbTe region		50	

Therefore, some different annealing methods were tested. In initial attempts (Method 1, Samples 1, 4, and 8, see Table 1), the samples were annealed with the clamp for the length of the annealing. It was, however, found that this decreased the cooling rate substantially as a lot of heat was retained in the steel clamps even after the quartz ampoule was quenched in water. The large diameter of the ampoule also decreased the heat transfer between the sample and the cooling water. In order to increase the cooling rate, the quartz glass was broken upon quenching in water (Method 2, samples 2, 9, and 10). However, since the samples are very fragile, diffusion couples were prone to cracking with this method due to thermal stresses caused by the rapid cooling. The remaining samples were bonded at 450 °C for 8 h. The heat treatment was terminated by inserting the ampoule into water without breaking it (Method 3, Samples 3, 5, 6, and 7). The diffusion contribution at this temperature and time scale was low.

The bonded couples were then resealed in quartz tubes with 10 mm diameter for annealing at various temperatures. As the diffusion couple was annealed in a smaller quartz tube without the presence of the steel clamp, the cooling rate is expected to be higher than that for Method 1, limiting diffusion during quenching. This diffusion, however, is difficult to avoid completely in Ag_2Te due to its superionic properties.

The samples were mounted on epoxy with conductive filler and were polished with SiC sandpaper (#240–800), alumina pastes (3–0.3 μm), and a colloidal silica solution (~0.05 μm). They were examined by FE-SEM with a backscatter electron detector for microstructures. The crystallographic orientations in the vicinity of the bonding interfaces were examined using the electron backscatter diffraction technique (EBSD; HKL Technology, Inc.). The operating voltage of the electron beam for EBSD was 20 kV. The surface of the samples was inclined at 70° to the vertical direction with respect to the electron beam. Electron backscatter patterns were analyzed using a commercial software package, Channel 5^{TM} (HKL Technology, Inc.). Chemical composition profiles were measured by electron probe microanalysis (EPMA) with wavelength dispersive detectors (JXA-8200, JEOL) with a 15 kV acceleration voltage and 30 nA of current. The spot sizes used for EPMA were chosen to be large enough to average the composition of the two-phase (matrix and precipitates) microstructure formed during cooling, and to be much smaller than the overall lengths of compositional variation by chemical diffusion. They are listed in Table 1. The PbTe sample that was prepared by unidirectional solidification by the Bridgman method and a piece of Ag were used as standards for ZAF correction [25] from X-ray intensities, Pb$M\alpha$, Te$L\alpha$, and Ag$L\alpha$, to compositions.

2.2. Unidirectional solidification by Bridgman method

Unidirectional solidification was performed on the composition $(PbTe)_{0.6470}(Ag_2Te)_{0.3529}$ (30 at% Ag). According to the reported phase diagram for the PbTe–Ag_2Te system [23], the primary solidification of this alloy should occur with PbTe phase. Elemental Pb, Te, and Ag (8 g in total) were sealed in a carbon coated quartz tube with an inner diameter of 6 mm under Ar atmosphere at 30 kPa. The sample was moved downwards in a Bridgman-type furnace holding 850 °C at a speed of 0.41 mm h^{-1}. The temperature gradient of the furnace was ~20 K mm^{-1} at temperatures around the eutectic temperature (~694 °C) [22,23]. The sample obtained from unidirectional solidification was cut in half in the longitudinal direction, mounted on a conductive epoxy, and polished in the same manner as the diffusion couples for observations by FE-SEM. The chemical composition was analyzed by EPMA with a 50 μm probe size to average the composition's heterophase microstructure.

3. Results and discussion

3.1. Phase assemblage and microstructure in diffusion couples

Fig. 2 shows the microstructure in the diffusion couple annealed at 650 °C for 1 h. No compositional contrast is observed in the regions far from the bonding Ag_2Te/PbTe interface on both sides (Fig. 2(d) and (e)). On the other hand, in the region close to the interface in the diffusion couple for which the annealing was terminated by quenching the ampoule in water without breaking the quartz tube, island shaped light phase is dispersed across a wide range on the Ag_2Te side (Fig. 2(a) and (b)), and plate shaped dark phase[2] is observed in the limited region in the vicinity of the

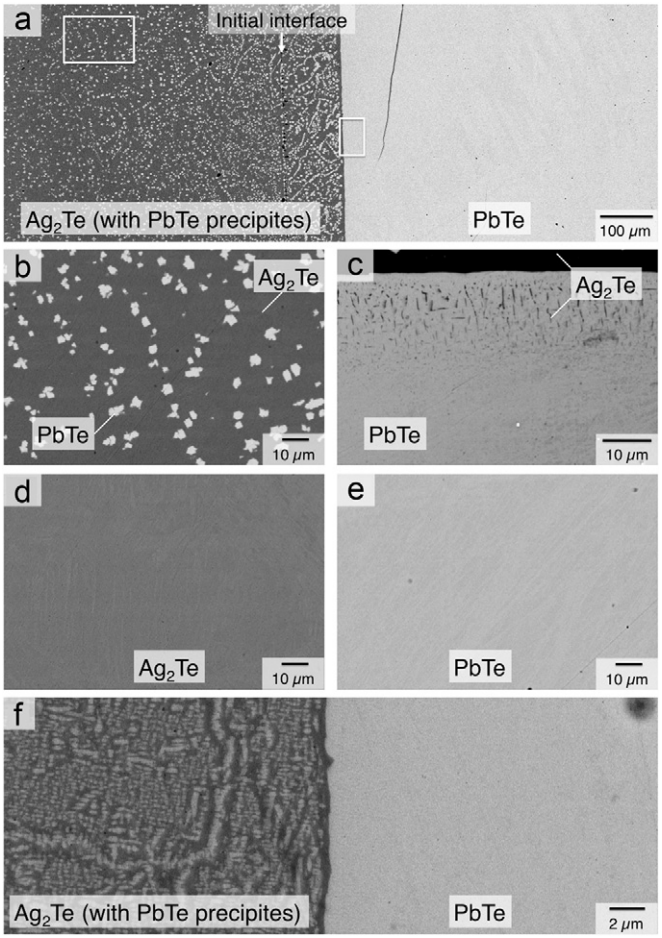

Fig. 2. Microstructures of PbTe/Ag_2Te diffusion couples annealed at 650 °C for 1 h by SEM in backscatter electron mode. The annealing runs were finished by quenching the whole ampoule in water without breaking the quartz tube (a–e) or by quenching the ampoule into water and immediately breaking the quartz tube (f). Figs. (a) and (f) show the Ag_2Te (with light PbTe precipitates)/PbTe interface. The regions delineated by white rectangles in (a) are enlarged in (b) and (c) (rotated 90° in clockwise). Figs. (d) and (e) show the regions far from the interface.

interface on the PbTe side (Fig. 2(a) and (c)). As Fig. 2 (a) and (d) shows, the volume fraction of the light phase in Ag_2Te is apparently larger at closer distances to the interface. Also, a comparison of the microstructures obtained using different cooling rates shows that the size of the microstructure is finer for (f) than (b); the spacing between precipitates is less than 1 μm in (f), while it is roughly ~10 μm in (b). For the diffusion couple in (f), annealing (650 °C, 1 h) was terminated by breaking the quartz tube in water, which is expected to result in a higher cooling rate. These observations suggest that the microstructure is formed due to solid state precipitation during cooling. Such fast diffusion during the short time period of cooling could be enabled by the very fast diffusion in α–Ag_2Te phase, which has superionic conduction capability. Therefore, for measurements of chemical composition profiles in the diffusion couples by EPMA, the electron beam spot sizes for individual samples shown in Table 1 were chosen so that they would be large enough to average the compositions of the two phases but quite small compared with the overall length of the variation of the average compositions.

Fig. 3 shows examples of composition profiles measured in the diffusion couples at various temperatures. No other phase than PbTe or Ag_2Te is formed in the examined temperature range of 375–650 °C, suggesting that no intermediate phase is stable in the system. This is consistent with the previous studies [22–24].

[2] In the zone on the PbTe side within a few micrometers of the PbTe/Ag_2Te interface, fewer precipitates are observed. In this zone, the solute is thought to have diffused into the Ag_2Te side during cooling instead of during precipitation.

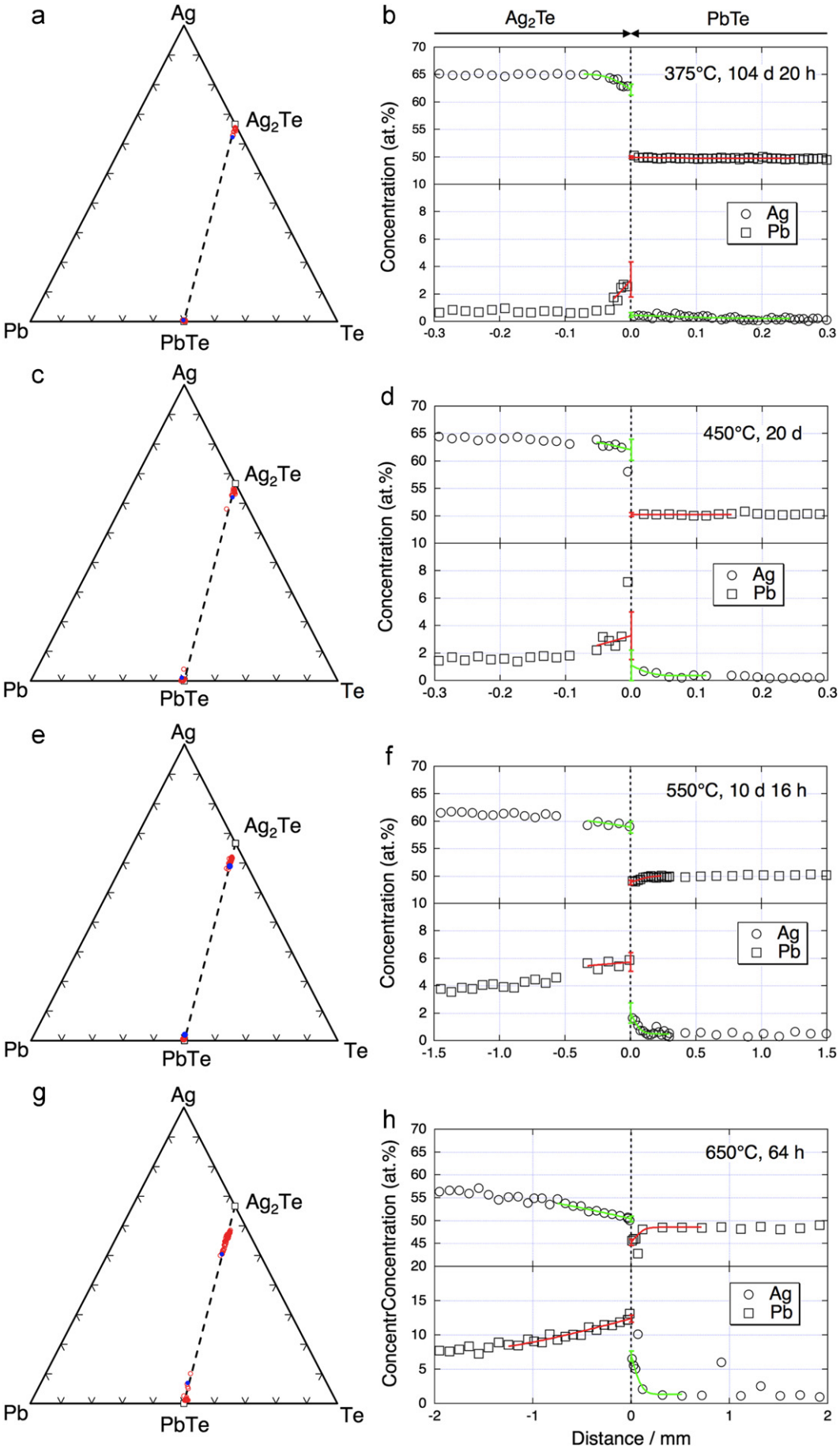

Fig. 3. Composition profiles obtained in the diffusion couples annealed under the conditions of 375 °C, 104 d 20 h (a and b), 450 °C, 20 d (c and d), 550 °C, 10 d 16 h (e and f), and 650 °C, 64 h (g and h). In the ternary plots (a, c, e, and g), the measured compositions are denoted by red circles, from which the phase boundary compositions (blue solid circles) are determined. Graphs on the right hand side (b, d, f, and h) show the compositions as functions of distance. Solid curves are fitted to experimental profiles resulting in the error range indicated by the bars at $x=0$ (the phase boundary). (For interpretation of the references to color in this figure legend, the reader is referred to the web version of this article.)

3.2. Determination of phase boundary compositions from diffusion couples

Assuming a local equilibrium condition is held, compositions at heterophase interfaces in diffusion couples should correspond to the phase boundary compositions in the equilibrium phase diagrams. However, phase boundary compositions determined by single-point measurements can contain systematic error because (1) chemical compositions vary as functions of position in general with the steepest gradient around the phase boundary and (2) the spatial resolution of chemical composition measurements is limited. Also, single-point measurements can contain significant statistic errors. In order to reduce errors as much as possible in the determination, we decided to fit curves to experimental profiles and extend them to the heterophase interface to determine the phase boundary compositions.

As Fig. 3 shows, all data points for compositions observed in diffusion couples are close to the pseudo-binary line. Uphill diffusion, which goes against a concentration gradient and is peculiar to systems composed of more than two elements, is not significant. This makes it possible to simplify the analysis as follows.

In general, a concentration profile from an interdiffusion experiment has a peculiar shape, exhibiting its steepest slope around the middle point and a gentler slope towards the edges. The following procedure is employed to obtain a good fitting to such concentration profiles. In cases where a diffusion couple is composed of two components that show a miscibility gap in the composition range $c^{\alpha}_{i,\mathrm{bound}}$–$c^{\beta}_{i,\mathrm{bound}}$ for the concentration for species i, and the diffusion coefficient D^{α}_{i} is assumed to be composition-independent, the concentration $c_i(x,\ t)$ at distance x from the phase boundary in the diffusion couple after annealing for time t is expressed as

$$\frac{c_i(x,t)-c_{i,0}}{c_{i,1}-c_{i,0}} = \frac{c^{\alpha}_{i,\mathrm{bound}}-c_{i,0}}{c_{i,1}-c_{i,0}}\left[1+\mathrm{erf}\left(\frac{x}{2\sqrt{D^{\alpha}_{i}t}}\right)\right] \quad (1a)$$

where $c_{i,0}$ and $c_{i,1}$ are the minimum and maximum concentrations of species i, respectively, in the diffusion couple for $x \le 0$ and $0 \le c_i(x,t) \le c^{\alpha}_{i,\mathrm{bound}}$. Similarly, for $x \ge 0$ and $c^{\beta}_{i,\mathrm{bound}} \le c_i\ (x,\ t) \le c_{i,1}$:

$$\frac{c_i(x,t)-c_{i,0}}{c_{i,1}-c_{i,0}} = 1-\left(1-\frac{c^{\beta}_{i,\mathrm{bound}}-c_{i,0}}{c_{i,1}-c_{i,0}}\right)\left[1-\mathrm{erf}\left(\frac{x}{2\sqrt{D^{\beta}_{i}t}}\right)\right] \quad (1b)$$

where D^{α}_{i} is the composition independent diffusion coefficient in the β phase [3]. In an actual case, since a diffusion coefficient is dependent on composition in some degree, Eqs. (1a) and (1b) are not expected to describe the whole variation of the concentration in a diffusion couple. However, a limited part of the concentration profile can be approximated by these equations. Therefore, in the present analysis, Eq. (1a) or (1b) was fitted to the experimental concentration profiles in the region close to the phase boundaries and extrapolated to the boundary positions to determine the phase boundary compositions. The range used in the fitting was selected so that the multiple correlation coefficient ($=R$) for the measured profile and fitted curve was higher than 0.9. However, for cases where the variation due to interdiffusion was small (<1 at%) and hence the scattering of measured concentrations was more significant, larger ranges of the concentration profiles were utilized in the fittings. Using Eq. (1a) or (1b), the errors arising from the extrapolation of the profiles to the phase boundary due to the peculiar shape of the concentration profiles were minimized.

Examples of this analysis are shown in Fig. 3, where the curves fitted using Eq. (1a) or (1b) are shown with experimental profiles. The fitted curves reproduce the experimental profiles reasonably well in their respective regions of fitting.

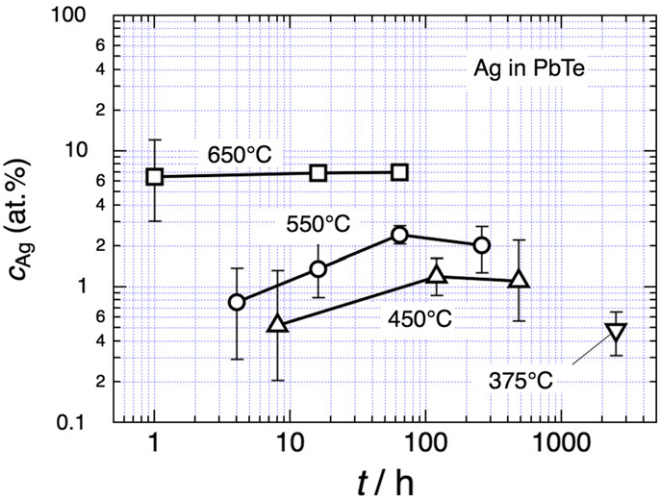

Fig. 4. Annealing time dependence of Ag solubility in PbTe at various temperatures determined by the diffusion couple experiments.

The phase boundary compositions thus determined should not depend on annealing time if they correspond to the equilibrium compositions. To check the validity of this theory, diffusion couples annealed for various time periods were analyzed. Fig. 4 shows the annealing time dependence of the heterophase interface compositions on the PbTe side at various temperatures. At 650 °C, no significant variation of the composition is found. At 450 and 550 °C, the variations of the composition are not significant for annealing lengths of 5 d and 64 h or longer, respectively. Therefore, in these periods, the heterophase interface compositions determined using the diffusion couples can be regarded as the equilibrium phase boundary compositions.

3.3. Unidirectional solidification by the Bridgman method

Unidirectional solidification by the Bridgman method under conditions with a steep temperature gradient and a slow velocity gives us useful information on phase diagrams, as has previously been demonstrated [26,27]. Fig. 5 shows microstructures of the sample with an initial composition of $(PbTe)_{0.6470}(Ag_2Te)_{0.3529}$ after it has been unidirectionally solidified by the Bridgman method. The total length of the sample is ~39 mm. The lower part is composed of PbTe matrix with Ag_2Te precipitates (Fig. 5(a) and (b)) and the upper part shows an eutectic structure composed of PbTe and Ag_2Te. The interface between the two regions is located at 17.8 mm.

The largest precipitates in the PbTe matrix (>1 μm) appear to take random shape (Fig. 5(a) and (b)) and are much larger in size than those observed in hot pressed samples after being held at 500 °C for 3 days [7] From Fig. 6(b), the compositions of these positions of Fig. 5(a) and (b) are ~7 and ~9 at% Ag, respectively. The solvus temperatures for these compositions are roughly 650 (~7 at% Ag) and 670 °C (~9 at% Ag) from Fig. 1. Therefore, in the sample prepared by the Bridgman method, the precipitation could start at higher temperature and hence be subject to coarsening more than in the hot pressed samples. Fine plate precipitates are also observed in the Bridgman sample as shown in the box of Fig. 5(b). These small precipitates could be formed at lower temperatures due to further lowering of solubility of Ag_2Te in PbTe.

Thus, the Ag_2Te precipitation in PbTe in the lower part of the rod proves that the solubility of Ag_2Te decreases with decrease in temperature. The primary solidification with PbTe phase is consistent with the reported phase diagram [23]. The decrease in the solubility of Ag_2Te in PbTe is consistent with the observation by Pei et al. [7]

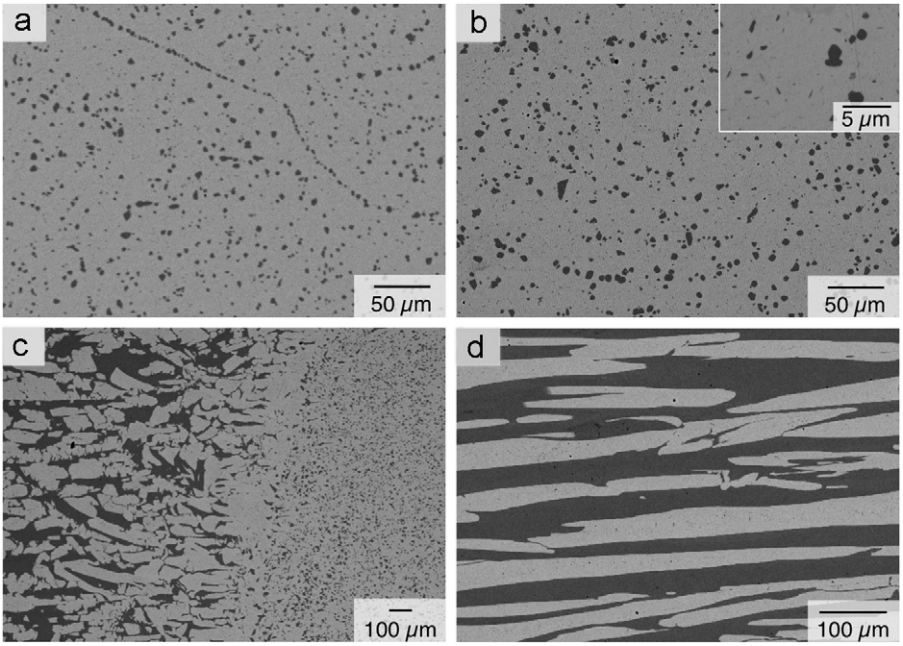

Fig. 5. Microstructure of the PbTe–Ag_2Te sample rod unidirectionally solidified by the Bridgman method in the PbTe region with Ag_2Te precipitates (distance from the bottom end of 2.1 mm (a) and 12.4 mm (b)), the interface of PbTe (with Ag_2Te precipitates), eutectic (17.8 mm) (c), and the eutectic microstructure region (above the interface (c)) (d). In all the images, the light region is PbTe phase and the dark region is Ag_2Te phase.

and the examination of solubility in the present work, which will be discussed in detail later. For the region of the PbTe matrix with Ag_2Te precipitates, the average compositions were measured by EPMA as functions of the distance from the bottom of the sample and are shown in Fig. 6. The compositions lie on the pseudo-binary PbTe–Ag_2Te line. The Ag concentration increases with increase in distance from the bottom of the sample. This is again expected from the phase diagram. As PbTe, which has a lower content of Ag than that in the melt solidifies the composition of the melt changes in the Ag-rich direction. Accordingly, the Ag content of the PbTe crystal increases. Eventually, the liquid composition reaches the eutectic composition and eutectic solidification begins. Since the Ag content is smaller in the lower positions (Fig. 6(b)), the volume fraction of Ag_2Te precipitate is smaller as well (Fig. 5(a) and (b)). The maximum Ag content in the PbTe phase, 14.9 ± 1.6 at% Ag, shown in Fig. 6(b) could correspond to the maximum solubility of Ag_2Te in PbTe at the eutectic temperature. Since interdiffusion in the longitudinal direction of the sample during cooling after solidification may have lowered the maximum Ag content in the sample, the maximum solubility in the equilibrium phase diagram could be equal or higher than the value determined above. The average composition of the region that exhibits the eutectic structure (Fig. 5(d)) is 43.4 ± 5.0% Ag. This composition should correspond to the eutectic composition of the equilibrium phase diagram and does not contradict previous data ($c_{Ag} \sim 47 \pm 1$ at% [23]).

3.4. Temperature dependence of solubility ranges of PbTe and Ag_2Te

In Fig. 1, the solubility ranges of both PbTe and Ag_2Te in the pseudo-binary PbTe–Ag_2Te system determined in this work are summarized including the data point determined through unidirectional solidification by the Bridgman method. For the solubility of Ag_2Te in PbTe, only one point has been measured at 500 °C previously [24].[3] The present data agree well with this point but are located at significantly lesser Ag concentrations than those on the curve drawn in the previous assessment [23]. For the solubility of PbTe in Ag_2Te, Wald [24] has drawn the dashed-dotted line in Fig. 1. The present solubility is slightly larger than that on the curve drawn by Wald. The reliability of Wald's curve is however limited as the line does not appear to coincide with his own experimental data points, showing a line with less solubility than the data indicate. Recently, the phase diagram of the pseudo-binary PbTe–Ag_2Te system has been calculated with the CALPHAD method [28]. The calculated phase diagram shows a liquid + PbTe + Ag_2Te region in the temperature range from ~450 to 700 °C. In the present work, no evidence of the existence of liquid phase was found in the diffusion couples, which show the compositional variation along the pseudo-binary line between PbTe and Ag_2Te as discussed in Section 3.2, at least up to 650 °C. Therefore, the parameters used in the calculation to describe the alloy system may need to be reconsidered.

The solubility of Ag_2Te in PbTe appears to be limited at low temperatures, but increases exponentially with temperature. While the solubility at the lowest temperature of the present work, 375 °C, is only 0.5 ± 0.2 at% Ag, the maximum solubility is 14.9 ± 1.6 at% Ag, as has been estimated from the Bridgman sample in Fig. 6. The solubility of PbTe in Ag_2Te also decreases remarkably with decrease in temperature. The temperature dependence of solubility is related to the thermodynamic properties of the system. For a moderately dilute solution in an eutectic binary system consisting of elements A and B where A and B form the α and β phases, respectively, with different crystal structures, the solubilities of B in the α phase, x_B^α, and A in the β phase, x_A^β, are expressed as functions of temperature T:

$$\ln x_{\mathrm{corr},B} \equiv \frac{1}{1-2x_B^\alpha} \ln\left(\frac{x_B^\alpha}{1-x_A^\beta}\right) = \frac{\Delta_f S_B}{R} - \frac{\Delta_n H_B}{RT}, \quad (2)$$

where R is the gas constant [29,30]. $\Delta_f S_B$ and $\Delta_n H_B$ are expressed as

$$\Delta_n H_B = \Delta_m H_B + \Delta H_B^{\beta\alpha}, \quad (3)$$

$$\Delta_f S_B = \Delta_e S_B + \Delta S_B^{\beta\alpha}, \quad (4)$$

[3] Although Wald [25] shows one more data point at ~700 °C, it is excluded here since the experimental procedure is not found in the paper.

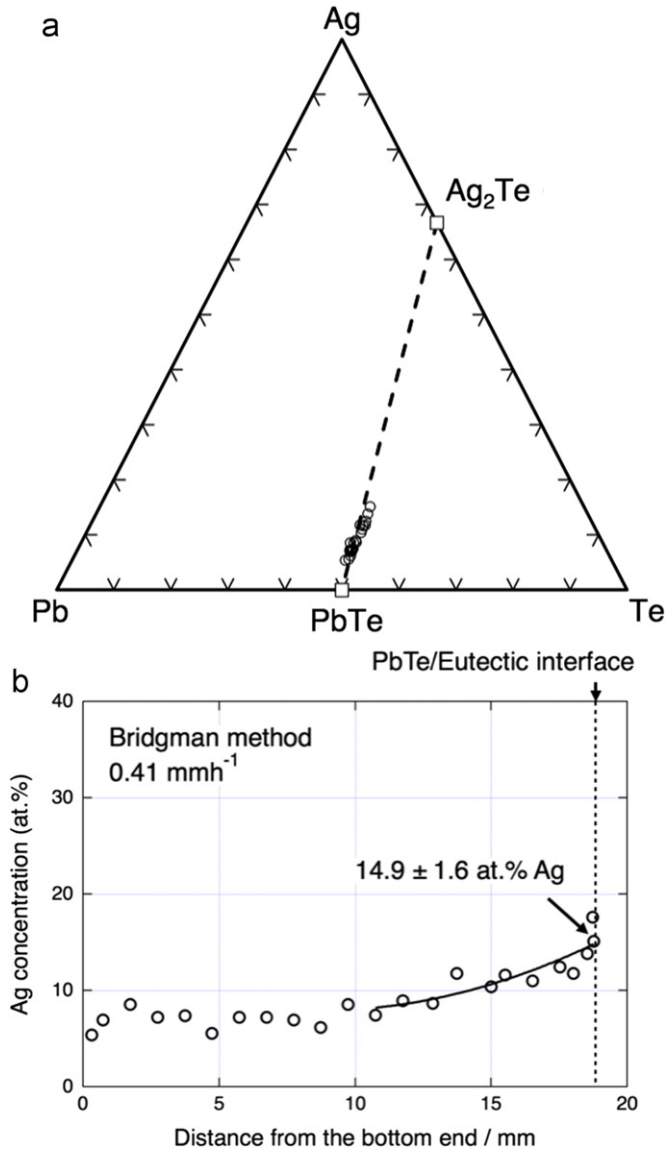

Fig. 6. Distribution of average compositions in the PbTe phase with Ag_2Te precipitates in a sample rod unidirectionally solidified by the Bridgman method and plotted in the Ag–Pb–Te ternary diagram (a) as a function of the distance from the bottom end of the rod (b). Squares indicate the ideal compositions of PbTe and Ag_2Te.

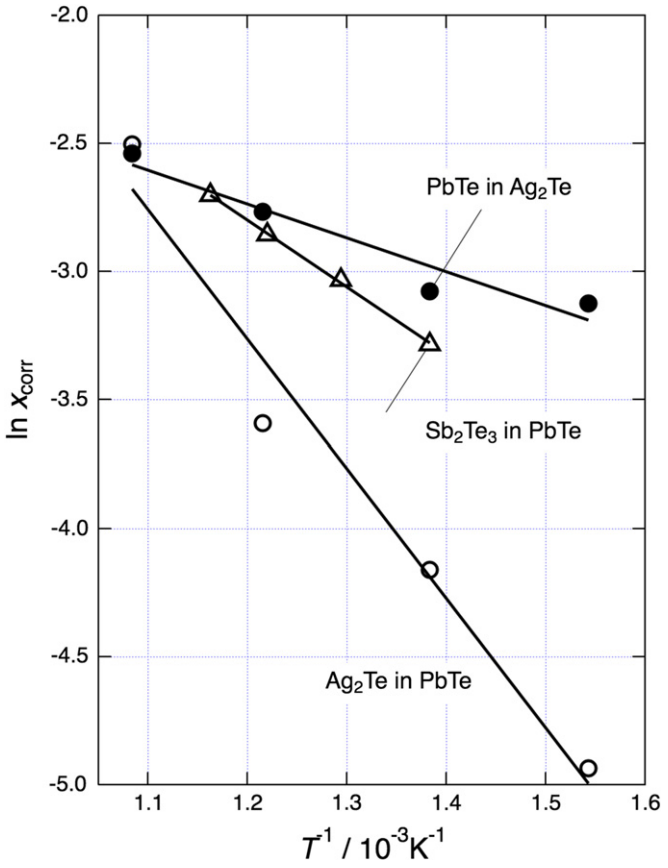

Fig. 7. Temperature dependence of the corrected composition at the solvus lines defined by Eq. (2) for the PbTe and Ag_2Te phases in the PbTe–Ag_2Te system (this work) and the PbTe phase in the PbTe–Sb_2Te_3 system [27]. Linear regression to the plots gives the heat of solution, Δ_nH_B, defined by Eqs. (2) and (3).

Table 2
The values of Δ_mH_B defined by Eq. (3) for dissolution of Ag_2Te in PbTe, PbTe in Ag_2Te, and Sb_2Te_3 in PbTe.

Solute	Matrix	Δ_nH_B (kJ mol^{-1})
Ag_2Te	PbTe	41.9 ± 10.6
PbTe	Ag_2Te	11.0 ± 4.3
Sb_2Te_3	PbTe	21.8 ± 1.0[a]

[a] Since the solubility of PbTe in Sb_2Te_3 is unknown, it is assumed to be zero ($x_A^{\beta}=0$ in Eq. (2)) in this estimation.

where Δ_mH_B is the partial molar enthalpy of mixing B in the α phase, Δ_eS_B is the excess partial molar entropy of mixing B in the A phase, and $\Delta H_B^{\beta\alpha}$ and $\Delta S_B^{\beta\alpha}$ are the molar enthalpy and entropy, respectively, required to change pure B from the β phase to the α phase. Here, we call Δ_nH_B the heat of solution. Therefore, the heat of solution for a binary system with differing crystal structures is composed of both mixing and phase change contributions.

Fig. 7 shows the plots of $\ln x_{corr}$ for the solubilities of PbTe in Ag_2Te and Ag_2Te in PbTe obtained in this work together with the plot of Sb_2Te_3 in PbTe [26] as functions of inverse temperature. For these pseudobinary systems, the molar fraction x_B was defined to be the atomic ratio belonging to the respective end members of the systems such as $(Pb_{0.5}Te_{0.5})_{1-xB}(Ag_{0.667}Te_{0.333})_{xB}$, $(Pb_{0.5}Te_{0.5})_{1-xB}(Sb_{0.4}Te_{0.6})_{xB}$, or $(Ag_{0.667}Te_{0.333})_{1-xB}(Pb_{0.5}Te_{0.5})_{xB}$. The negative slopes of these plots imply that the dissolution reaction is endothermic. The plots show straight lines for all of these systems. For this reason, lines are fitted to these plots by a least squares method resulting in the molar enthalpies due to mixing and phase change (Eq. (3)) listed in Table 2.

3.5. Heat of solution

Among the combinations of the solute and matrix phases listed in Table 2, Δ_nH_B for Ag_2Te dissolution in PbTe is significantly larger than that for the others. For isostructural systems, in general, four main factors could affect the heat of solution: (1) size difference, (2) covalency (ionicity) difference, (3) valence, and (4) electron configuration [31]. Of these, size difference, which causes strain in the crystal, is generally the most important [31,32]. In addition to these factors, for non-isostructural systems, defect structure needs to be considered.

Here we first compare the dissolution of Ag_2Te and Sb_2Te_3 in PbTe. In the solid solution PbTe in the pseudobinary PbTe–Ag_2Te system, it has been suggested that half of the Ag atoms occupy interstitial sites while donating one electron and compensate for the remaining Ag substituting for Pb atoms [4,7]. This means that one interstitial defect and one substitutional defect are introduced per dissolution of three atoms of Ag_2Te. In dissolution of

Sb_2Te_3 in PbTe, Sb^{+3} substitutes for Pb^{2+} [33] introducing a vacancy on a Pb^{2+} site. Therefore, one vacancy and two substitutional defects are likely formed per dissolution of five atoms of Sb_2Te_3. Comparing these two cases, the total number of point defects introduced per dissolution of one solute atom is slightly larger for Ag_2Te dissolution (0.667) than Sb_2Te_3 (0.6). The Shannon ionic radius of Ag^+ (0.115 nm [34]) is similar to that of Pb^{2+} (0.119 nm [34]), while that of Sb^{3+} (0.076 nm [34]) is significantly smaller. Therefore, the size effect cannot explain the larger $\Delta_n H_B$ of Ag_2Te dissolution. Covalency is related to electronegativity. The electronegativities for Pb, Te, Sb, and Ag are 3.08, 3.59, 3.34, and 2.59, respectively, by Sanderson's definition[4] [36]. The difference in Pb–Ag electronegativities is larger than that of Pb–Sb. The higher energy of dissolution of Ag_2Te in PbTe could be attributed to the difference in the bonding character. The present result is also qualitatively consistent with an *ab initio* calculation study that predicts the energy to replace a Pb atom on a Pb site with an Ag atom is 0.6371 eV, while that to replace a Pb atom on a Pb site with a Sb atom is 0.4028 eV [37]. Thus, the substitution of Pb with Ag requires more energy than substitution with Sb.

Ag_2Te is in the β-phase ($145\ ^\circ C < T < 802\ ^\circ C$ [11]) and shows superionic conductivity in the temperature range of the present solubility measurements [9,10]. In this phase, silver ions randomly occupy both the tetrahedral and octahedral sites in a tellurium face-centered cubic structure, leaving these sites only partially filled [12], causing the fast Ag^+ ion conduction. The radius of Pb^{2+} ions is similar to that of Ag^+, as mentioned above. It is therefore likely that Pb^{2+} ions behave in a similar manner to Ag^+ ions. Since there are many unoccupied sites for Ag^+ ions, the additional energy to place Pb^{+2} ions in those sites is expected to be small. This could lead to the small heat $\Delta_m H_B$ for PbTe dissolution in Ag_2Te.

It should be noted that the driving force of precipitation is related to the heat of solution [38]; the chemical driving force for nucleation ΔG_{chem} is expressed as

$$\Delta G_{chem} = -\Delta H_s(\Delta T/T_s), \quad (5)$$

where ΔH_s is the heat of solution, ΔT is supercooling, and T_s is the solvus temperature. Larger heat of solution leads to larger chemical driving force of precipitation and contributes to higher nucleation rates. In the present cases, $\Delta_n H_B$ in Eq. (3) is regarded as the heat of solution ΔH_s.

Therefore, it is expected that among the precipitation of Ag_2Te in PbTe, PbTe in Ag_2Te, and Sb_2Te_3 in PbTe, Ag_2Te precipitation in PbTe matrix will gain the largest contribution to the driving force of nucleation from the heat of solution. In order to discuss the nucleation rate of precipitation quantitatively, one also needs to take into account the strain and interfacial energies associated with the precipitation and diffusivities of atoms. However, the evaluation of these quantities is beyond the scope of this work. Also, the microstructures one observes after heat treatments reflect a coarsening process to some degree in addition to the nucleation process. Here, we attempt to make a rough comparison of the number density of precipitates for the three cases. It is obvious from Fig. 2 that the number density of Ag_2Te precipitates in PbTe is higher than that of PbTe precipitates in Ag_2Te, matching the larger chemical driving force expected from Eq. (5). For Ag_2Te and Sb_2Te precipitates in PbTe, there are quantitative data on the number density as shown in Table 3. In this comparison, the annealing conditions were picked to give a similar degree of supercooling ($\Delta T/T_s$). The number density of Ag_2Te precipitates, $55 \pm 30\ \mu m^{-3}$, is significantly higher than that for Sb_2Te_3 precipitates, $15 \pm 3\ \mu m^{-3}$.

[4] Sanderson's definition is chosen here because it can illustrate the anomaly in the electronegativities of the posttransition elements [35].

Table 3
Chemical driving force for the precipitation ($-\Delta_n H_B(\Delta T/T_s)$, Eq. (2), and number density of precipitates of Ag_2Te and Sb_2Te_3 in PbTe after isothermal annealing.

Precipitate	Annealing condition	T_s (°C)	ΔT (K)	$\Delta T/T_s$	$-\Delta_n H_B(\Delta T/T_s)$ (kJ mol^{-1})	N_V (μm^{-3})	Ref. for N_V
Ag_2Te	500 °C 3 d	~630[a]	130	0.144	−6.0	55 ± 30	[7]
Sb_2Te_3	450 °C 38 h	~575[b]	125	0.147	−3.2	15 ± 3	[45]

[a] Evaluated from the solvus determined in this work.
[b] Evaluated from the solvus reported in [27].

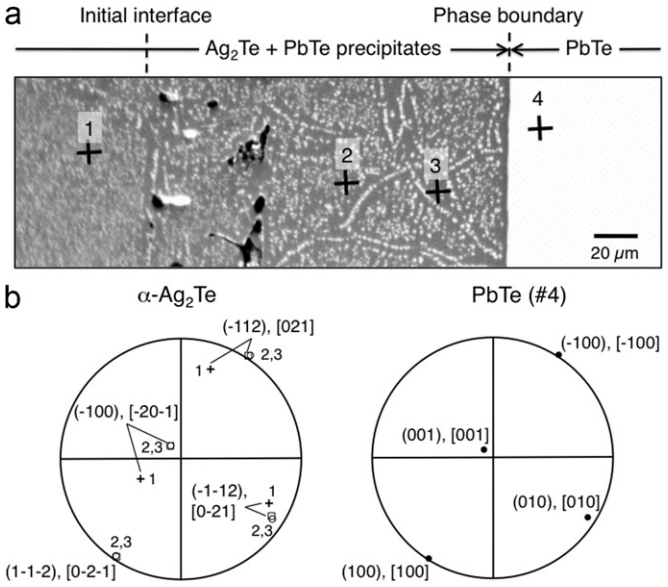

Fig. 8. The microstructure in the vicinity of the initial interface and phase boundary in the diffusion couple annealed at 550 °C for 16 h after diffusion bonding at 450 °C for 8 h (a). The EBSD measurements have been performed at the points shown in (a) resulting in the pole figures for planes and directions of α-Ag_2Te (for points 1–3 in (a)) and PbTe (for point 4 in (a)) shown in (b). The number indicated in (b) corresponds to the point number in (a). The points for 2 (□) and 3 (○) (in the region between the initial interface and the phase boundary, where PbTe phase transformed to Ag_2Te phase during annealing) and 4 (in the PbTe phase region) are located close to each other in the pole figures.

3.6. Phase growth and chemical diffusion behavior in the diffusion couples

In all the diffusion couples, the Ag_2Te phase grew into the PbTe phase as shown in Fig. 2(a). This can be understood as a result of the fact that the solubility of PbTe in Ag_2Te is larger than that of Ag_2Te in PbTe. This experimental fact implies that, in the region between the phase boundary and the initial interface, the PbTe crystal has transformed into α-Ag_2Te crystal during annealing and then the newly formed β-Ag_2Te has transformed to α-Ag_2Te at ~145 °C [11] upon cooling after annealing. To examine the orientation relationship among the original PbTe phase, newly formed Ag_2Te phase, and original Ag_2Te phase, an EBSD experiment has been performed. Electron backscatter patterns were collected at the four points shown in Fig. 8(a). Points 2 and 3 are located in the newly formed Ag_2Te phase while point 1 is in the original Ag_2Te region. Point 4 is in the PbTe region, which is close to points 2 and 3. Fig. 8(b) shows that the crystal orientation of the newly formed Ag_2Te phase (points 2 and 3) is correlated to that of PbTe (point 4), while that from the original Ag_2Te region (the point 1) is not. The orientation relationship between point 4 from PbTe (cubic, space group: *Fm*-3*m*) and points 2 and 3 from the α-Ag_2Te crystal (monoclinic, space group: $P2_1/c$) that has transformed from PbTe is {111} of PbTe//(−100), (1−1−2),

$(-1-12)$ of α-Ag_2Te, and 〈001〉 of PbTe//[−20−1], [0–2–1], [0–21] of β-Ag_2Te. Since the transformation from the high temperature cubic β-Ag_2Te to the low temperature α-Ag_2Te requires only small local atomic shifts because of the relationship between cubic β- and monoclinic α-Ag_2Te crystals [39], at high temperature the β-Ag_2Te crystal should possess a cube-on-cube relationship with PbTe. This orientation relationship is the same as that observed between Ag_2Te precipitates and PbTe matrix [8] or $AgSbTe_2$ [40] matrix, and for the transformation between α- and β-Ag_2Te [39]. Thus, the region in the diffusion couple where PbTe has transformed to Ag_2Te due to the chemical composition change maintains the crystal orientation before the transformation but does not have a crystallographic orientation relationship with the Ag_2Te phase from which the transformation grew. The present result suggests that the transformation from PbTe to B-Ag_2Te occurs via the change in chemical composition on the cation sublattice in PbTe. The precipitation of Ag_2Te in PbTe and the transformation from PbTe to Ag_2Te in a diffusion couple are expected to be different in some viewpoints, such as stress distribution and ratio of interfacial area to volume. The fact that the same orientation relationship as the precipitation of Ag_2Te was confirmed in a diffusion couple gives an insight into the precipitation mechanism in PbTe.

Interestingly, precipitates of PbTe in Ag_2Te in the region close to the phase boundary (Fig. 8(a)) are partly aligned, forming a grain boundary-like structure. While this suggests that there is a substructure, it should not be with grain boundaries in the usual sense but could be with small angle tilt boundaries since EBSD gives similar orientations for the two points belonging to different cells. Because of faster atomic diffusion along the boundaries and/or smaller energy requirements for nucleation of precipitates due to the defective nature of the boundaries, the precipitates could preferentially be formed on them.

Four independent interdiffusion coefficients can be defined for interdiffusion in a ternary system. At least two such diffusion couples with differing compositions of the end members giving a cross point on a ternary diagram are needed to measure interdiffusion coefficients [41]. In this work, we do not determine interdiffusivities but instead give qualitative insight into the diffusion behavior in this system.

As seen in Fig. 3, the slope of the concentration profiles of Pb in Ag_2Te is gentler than that of Ag in PbTe. This means that the interdiffusivity in Ag_2Te is higher than that in PbTe. Ag_2Te is a superionic conductor in the temperature range used in this work [9,10]. The cause of the fast diffusion can be explained by Ag^+ ions diffusing in both octahedral and tetrahedral sites in the tellurium fcc base structure [12]. Interdiffusion in a pseudobinary ionic compound system is subject to the constraint of electroneutrality; for cases where anion diffusion is much slower than cation diffusion, interdiffusivity is dominated by the diffusion of the slower cation [42]. In Ag_2Te, the diffusivity of Te^{-2} is much slower than that of Ag^+ [14]. Therefore, the interdiffusivity is expected to be dominated by the diffusion of the slower cation: either Ag^+ or Pb^{+2}. In either case, the high interdiffusivity observed in the present study suggests that Pb^{+2} is also a very fast diffuser in the Ag_2Te phase. The size of the Pb^{2+} ions is similar to that of the Ag^+ ions, as discussed above. It is therefore possible that Pb^{2+} ions diffuse in a similar manner to the fast-diffusing Ag^+ ions. In Ag_2Te phase in the diffusion couples, precipitates are formed during cooling. Such fast formation of precipitates could be attributed to the high interdiffusivity of β-Ag_2Te.

4. Conclusions and remarks

The solvus lines of the PbTe phase and Ag_2Te phase in the pseudobinary PbTe–Ag_2Te system have been determined by diffusion couple experiments and a unidirectional solidification experiment. The solubilities of both Ag_2Te in PbTe and PbTe in Ag_2Te decrease with decrease in temperature from 14.9 at% Ag (694 °C) to 0.5 at% Ag (375 °C) for the Ag_2Te dissolution in PbTe and from 12.4 at% Pb (650 °C) to 3.1 at% Pb (375 °C) for the PbTe dissolution in Ag_2Te. The decrease in solubilities leads to the formation of precipitates of Ag_2Te in PbTe and PbTe in Ag_2Te during cooling for saturated solutions. In particular, the fast atomic diffusion in Ag_2Te results in the precipitation of PbTe even in quenched samples. From the temperature dependence of solubilities, heats of solution have been determined. The larger heat of solution for the Ag_2Te dissolution in PbTe than that for the Sb_2Te_3 dissolution in PbTe determined based on previous experimental data results in the formation of Ag_2Te precipitates in PbTe with a larger number density than Sb_2Te_3 precipitates in PbTe. In the diffusion couple, the phase boundary moves toward PbTe. In the region between the phase boundary and the initial interface, PbTe transforms to β-Ag_2Te (cubic) while retaining the cube-on-cube orientation relationship.

When attempting to reduce the lattice thermal conductivity of thermoelectric materials, it is important to control the size scale of the microstructure, especially the interfacial area per unit volume [43]. For microstructures with plate precipitation of bulk materials, this can be done through control of the number density of precipitates on the basis of nucleation theories [44]. In a previous paper [44], it has been shown that the number density of precipitates can be controlled through several parameters (temperature and time in cases of isothermal heat treatments, and cooling rate and concentration of solute in cases of cooling heat treatments) in a given material system. In this paper, we emphasize that the heat of solution should be taken into account in selecting the material system. There are three energies in the expression describing nucleation rate that could be manipulated: interfacial energy, strain energy, and chemical driving force [45]. There is a typical range for interfacial energies that many material combinations fall into: 0.2–0.8 for semicoherent interfaces and 0.8–2.5 $J\,m^{-2}$ for incoherent interfaces [46]. In an analogous way, we could expect some typical range for strain energies because very high strain energy would trigger some kind of relaxation mechanism. In contrast, chemical driving force, ΔG_{chem}, which is expressed using the heat of solution for cases of precipitation as in Eq. (5), can vary from negative to positive values depending on the material system. We would expect manipulating the heat of solution to have a large impact on the number density of precipitates.

Acknowledgments

We would like to thank Nathan Marolf for help in sample preparations, Professor Hiroshi Okuda of Kyoto University for fruitful discussion, and Jessica Swallow for proofreading. This work was funded by the PRESTO program (PRESTO: Precursory Research for Embryonic Science and Technology) of Japan Science and Technology Agency. Microscopy facilities are supported by NSF CSEM MRSEC at Caltech.

References

[1] M.G. Kanatzidis, Chem. Mater. 22 (2010) 648–659.
[2] J.M. Ziman, Electrons and Phonons: The Theory of Transport Phenomena in Solids, Oxford University Press, Oxford, 1960.
[3] P. Shewmon, Diffusion in Solids, 2nd Edn., Wiley, Warrendale, PA, 1989.
[4] A.J. Strauss, J. Electr. Mater 2 (1973) 553–569.
[5] M. Battaglioli, V. Fano, G. Mignoni, R. Pergolari, in: 4th International Conference on Thermoelectric Energy Conversion (ICTEC), 1982, p. 114.
[6] Y. Noda, M. Orihashi, I.A. Nishida, Mater. Trans. JIM 39 (1998) 602–605.
[7] Y. Pei, J. Lensch-Falk, E.S. Toberer, D.L. Medlin, G.J. Snyder, Adv. Funct. Mater. 21 (2011) 241–249.

[8] J.L. Lensch-Falk, J.D. Sugar, M.A. Hekmaty, D.L. Medlin, J. Alloys Compd 504 (2010) 37–44.
[9] S. Miyatani, J. Phys. Soc. Jpn. 13 (1958) 341–350.
[10] H. Okazaki, J. Phys. Soc. Jpn. 43 (1977) 213–221.
[11] I. Karakaya, W.T. Thompson, Binary Alloy Phase Diagrams, in: T.B.M. (Chief), H. Okamoto, P.R. Subramanian, L. Kacprzak, J. William, W. Scott (Eds.), ASM International, Materials Park, Ohio, 1990, pp. 101–103.
[12] D.A. Keen, H. Stephen, J. Phys.-Condes. Matter 10 (1998) 8217–8234.
[13] M. Kobayashi, K. Ishikawa, F. Tachibana, H. Okazaki, Phys. Rev. 38B (1988) 3050–3055.
[14] C. Wood, V. Harrap, W.M. Kane, Phys. Rev. 121 (1961) 978–982.
[15] S.A. Aliev, U.K. Suyunov, D.G. Arasly, M.I. Aliev, Sov. Phys. Semicond. 7 (1973) 737–740.
[16] S.A. Aliev, E.I. Nikulin, Inorg. Mater. 13 (1977) 607–608.
[17] O.P. Astakhov, V.D. Golyshev, Inorg. Mater. 10 (1974) 1931–1934.
[18] M. Fujikane, K. Kurosaki, H. Muta, S. Yamanaka, J. Alloys Compd. 393 (2005) 299–301.
[19] M. Fujikane, K. Kurosaki, H. Muta, S. Yamanaka, J. Alloys Compd. 387 (2005) 297–299.
[20] K.F. Hsu, S. Loo, F. Guo, W. Chen, J.S. Dyck, C. Uher, T. Hogan, E.K. Polychroniadis, M.G. Kanatzidis, Science 303 (2004) 818–821.
[21] B.A. Cook, M.J. Kramer, J.L. Harringa, M.-K. Han, D.-Y. Chung, M.G. Kanatzidis, Adv. Funct. Mater. 19 (2009) 1–6.
[22] R. Blachnik, B. Gather, J. Less-common Met. 60 (1978) 25–32.
[23] B. Grieb, E. Lugscheider, J. Wilden, Ternary Alloys, VCH, 1988, pp. 465–476.
[24] F. Wald, J. Less-common Met. 13 (1967) 579–590.
[25] P.E.J. Flewitt, R.K. Wild, Physical Methods for Materials Characterization, Institute of Physics Publishing, Bristol and Philadelphia, 1994.
[26] T. Ikeda, V.A. Ravi, G.J. Snyder, Acta Mater. 57 (2009) 666–672.
[27] T. Ikeda, M.B. Toussaint, K. Bergum, S. Iwanaga, G.J. Snyder, J. Mater. Sci. 46 (2011) 3846–3854.
[28] W. Gierlotka, J. Łapsa, K. Fitzner, J. Phase Equilib. Diff. 31 (2010) 509–517.
[29] J.F. Freedman, A.S. Nowick, Acta Metall. 6 (1958) 176–183.
[30] J.W. Christian, The Theory of Transformations in Metals and Alloys, Pergamon, 2002.
[31] P.K. Davies, A. Navrotsky, J. Solid State Chem. 46 (1983) 1–22.
[32] R.A. Swalin, Thermodynamics of solids, John Wiley & Sons, Inc., New York, 1962.
[33] P. Zhu, Y. Imai, Y. Isoda, Y. Shinohara, X. Jia, G. Zou, J. Phys.: Condens. Matter 17 (2005) 7319–7326.
[34] R.D. Shannon, Acta Crystallogr. 32A (1976) 751–767.
[35] J.E. Huheey, Inorganic Chemistry—Principles of Structure and Reactivity, 2nd edition, Harper and Row, New York, 1978.
[36] R.T. Sanderson, Chemical Bonds and Bond Energy, Academic Press, New York, 1971.
[37] S.V. Barabash, V. Ozolins, C. Wolverton, Phys. Rev. 78B (2008) 214109.
[38] K.C. Russell, Adv. Colloid Interface Sci. 13 (1980) 205–318.
[39] C. Manolikas, J. Solid State Chem. 66 (1987) 1–6.
[40] J.D. Sugar, D.L. Medlin, J. Alloys Compd. 478 (2009) 75–82.
[41] J.S. Kirkaldy, Diffusion in the Condensed State, Institute of Metals, London, 1987.
[42] M.-F.S. Tang, D.A. Stevenson, J. Phys. Chem. Solids 51 (1990) 563–569.
[43] M.-S. Jeng, R. Yang, D. Song, G. Chen, J. Heat Transfer 130 (2008) 042410.
[44] T. Ikeda, N.J. Marolf, K. Bergum, M.B. Toussaint, N.A. Heinz, V.A. Ravi, G.J. Snyder, Acta Mater. 59 (2011) 2679–2692.
[45] R.D. Doherty, in: R.W.C.a.P. Haasen (Ed.), Physical Metallurgy, Elsevier Science, Amsterdam, 1996, p. 1364.
[46] J.M. Howe, Interfaces in Materials, John Wiley & Sons, Inc., New York, 1997.